Towards an efficient multiscale modeling of low-dimensional reactive systems: Study of numerical closure procedures

Giacomo Mazzi,[1] Yannick De Decker,[2] and Giovanni Samaey[1,a)]
[1]*Scientific Computing, Department of Computer Science, KU Leuven, Leuven, Belgium*
[2]*Interdisciplinary Center for Nonlinear Phenomena and Complex Systems (CENOLI), Université Libre de Bruxelles, Bruxelles, Belgium*

(Received 19 April 2012; accepted 12 October 2012; published online 27 November 2012)

We study a numerical closure approach for systems of chemical reacting systems on lattices with low-dimensional support, for which a mean-field approximation is insufficiently accurate because of lateral interaction on the lattice. We introduce a hierarchy of macroscopic state variables, taking particle clusters into account, whose time evolution is obtained via microscopic (kinetic Monte Carlo) simulation. The macroscopic state variables are chosen such that can be straightforwardly conserved during reconstruction of a microscopic configuration (the so-called lifting step). We present and compare the effects of different alternatives to initialize the remaining degrees of freedom. We illustrate the strong interplay between the number of macroscopic state variables and the specifics of the lifting and that, for a given lifting operator, accuracy of the macroscopic dynamics does not necessarily improve monotonically when adding macroscopic state variables. © *2012 American Institute of Physics*. [http://dx.doi.org/10.1063/1.4764109]

I. INTRODUCTION

Chemically reacting systems on low-dimensional spatial structures, such as a lattice, are frequently encountered, e.g., when modeling catalytic reactions on surfaces. In such cases, a mean field approximation, expressing the law of mass action for the species concentrations, is insufficiently accurate, since low-dimensional structure of the lattice inhibits mixing and increases the importance of local structure.[1,2] While for specific model problems, it may be possible to obtain a more accurate macroscopic description, e.g., by taking pair correlations into account,[3] such analytic closure approximations depend strongly on the system considered. Also, when more additional variables are needed, the equations quickly become intractable. An alternative is then to resort to a more microscopic individual-based stochastic simulation, such as a kinetic Monte Carlo model.[4,5] These simulations are especially powerful when combined with density functional theory or *ab initio* methods.[6] This allows for the introduction of realistic elementary mechanisms and associated energy barriers in the transition probabilities they are based on. There are nowadays many examples of successful applications of such advanced simulations, which open the way to a realistic modeling and interpretation of complex surface reactions,[7] but this increased realism has a cost: simulations become computationally more and more expensive, so that their acceleration becomes highly desirable (if not mandatory).

Currently, computational strategies are being studied that accelerate such individual-based particle simulations by introducing on-the-fly *numerical* closures: we mention equation-free[8,9] and heterogeneous multiscale methods (HMM).[10,11] In both approaches, the crucial steps are (i) to obtain a set of macroscopic state variables that are sufficient to drive evolution and (ii) to define an operator that generates a microscopic state corresponding to a given macroscopic state. This second step is equivalent to prescribing the closure approximation; in the equation-free, respectively, HMM, frameworks, this step is called lifting, respectively, reconstruction. The converse operator (mapping a microscopic state to a macroscopic one) is called restriction. Once these operators are available, one can construct a *coarse time-stepper*, which evolves the chosen macroscopic state variables over some time interval by means of a three-step procedure: (i) lifting; (ii) microscopic simulation; and (iii) restriction.

Equation-free methods have already been used to perform numerical bifurcation analysis of lattice chemical systems.[12,13] In Ref. 12, one studies a CO oxidation process on a lattice. Here, a kinetic Monte Carlo method exhibits a bistability observed which cannot be fully captured by an explicit macroscopic closure. Nevertheless, using a coarse time-stepper with only species concentrations as macroscopic state variables (but with a different lifting operator, a different numerical closure), the observed macroscopic bistability can be completely explained. For a similar study for NO reduction by CO over a Pt(100) surface, see Ref. 13. In both cases, the lifting equilibrates the lattice by exploiting a separation in time scales between (fast) diffusion on the lattice and (slower) chemical reactions, allowing incorrectly initialized higher order correlations to quickly relax ("heal") to a correct functional of the species concentrations. Generalized constrained simulation algorithms have been proposed to enforce healing when the chosen macroscopic observables also contain fast components.[14,15]

The present paper studies lifting/reconstruction techniques in situations where the "healing effect" is absent due

a)Author to whom correspondence should be addressed. Electronic mail: giovanni.samaey@cs.kuleuven.be.

 © 2012 American Institute of Physics

to a lack of time-scale separation. In particular, we investigate chemically reacting systems in a crowded environment that makes diffusion ineffective. As already pointed out in Ref. 12, two problems are expected: (i) additional macroscopic state variables will be needed and (ii) without clear time-scale separation, lifting artifacts will not heal completely. Additionally, whereas[12,13] only considered steady-state behavior, we are also interested in recovering (transient) macroscopic dynamics.

The main contributions of the present paper are twofold. From an algorithmic viewpoint, we develop a numerical closure strategy to recover the macroscopic (transient) dynamics of two specific chemical systems with nonlinear reactions, defined in Sec. II. We introduce a hierarchy of macroscopic state variables for which a consistent lifting operator can be implemented (Sec. III) and consider several options to initialize the remaining degrees of freedom (Sec. IV). From a computational physics viewpoint, we analyze the effect of the different lifting strategies (corresponding to different closure approximations) on macroscopic evolution (Sec. V). We show that both the number and type of macroscopic state variables and the choice of lifting operator (for given macroscopic state variables) can significantly affect the observed macroscopic evolution and, hence, the accuracy of the multiscale approach. The study is restricted to one-dimensional systems, not only for simplicity but also because low dimensionality effects are more pronounced in one space dimension.

II. CHEMICAL REACTIONS ON A RING

We consider a ring with N lattice sites. Each lattice site is occupied by exactly one particle of species A or X. The dynamics of the system is governed by a set of I reactions, with associated reaction rates k_i $(1 \leq i \leq I)$. Reactions can only occur if the reacting particles are in adjacent sites. We adopt a slight modification of the notations that were introduced in, e.g., Refs. 16–18: we define the microscopic state at time t as $\boldsymbol{\sigma}(t) = \{\sigma_1(t), \sigma_2(t), \ldots, \sigma_N(t)\}$ with each $\sigma_n(t) = \pm 1$, depending on whether the lattice site n is occupied by A $(\sigma_n(t) = +1)$ or X $(\sigma_n(t) = -1)$. We also define the coverage of species A as

$$a(t) := \frac{1}{2}\left(\frac{1}{N}\sum_{n=1}^{N}\sigma_n(t) + 1\right). \tag{1}$$

Correspondingly, $x = 1 - a$ is the coverage of species X.

We consider two particular example systems:

Example 2.1 (Schlögl model). We consider Schlögl's second model,[18] in which the reactions are given as

$$\begin{aligned} XAX &\underset{k_2}{\overset{k_2}{\rightleftharpoons}} XXX, \\ X &\underset{k_4}{\overset{k_3}{\rightleftharpoons}} A, \end{aligned} \tag{2}$$

where the notation in the first line is chosen to emphasize that only elements surrounded by two X may react. This model is widely used as a prototype non-equilibrium system on constrained configurations, such as catalytic reactions on surfaces.[19,20] Similar equations have been proposed to describe disease spreading in epidemic models.[21]

Example 2.2 (Simple trimolecular reaction). We may simplify the above prototypical example even further by only retaining the trimolecular reaction, i.e.,

$$XAX \underset{k_2}{\overset{k_2}{\rightleftharpoons}} XXX, \tag{3}$$

where we assume $k_1 = k_2 = 1$. This model contains the simplest mechanism to obtain a macroscopic behavior that nontrivially depends on the local configurations.[17,22] Note that this example arises as the limit of Schlögl's second model when $k_3 = k_4 = 0$.

We simulate individual realizations of the above stochastic processes via a kinetic Monte Carlo (kMC) method with an accept-reject strategy (a so-called null-event kMC, see, e.g., Refs. 5 and 23) and propensity functions that depend on the lattice site; see Refs. 17 and 22 for algorithmic details.

Starting from the master equation, describing the deterministic evolution of the probability distribution of the realizations over the configuration space,[1,16] a number of approximate macroscopic models have been proposed. The simplest one is the mean-field approximation, where, by substituting all the high order correlations with an average (mean field) interaction, one writes a set of ordinary differential equations for the coverages.[18,24] More accurate models take pair correlations into account via the Ursell expansion.[25] Alternatively, the Kirkwood approximation[26] and the Bethe-type ansatz[18] express high order moments directly as functionals of the lower ones. Despite the simplicity of the considered models, however, the derivation and analysis of higher order approximations quickly becomes quite tedious and intricate.

III. NUMERICAL CLOSURE ALGORITHM

We now describe the numerical closure algorithm that is the focus of the present paper. We first define a hierarchy of macroscopic state variables (Sec. III A). We then introduce numerical *lifting* and *restriction* procedures to map macroscopic to microscopic states, and vice versa (Sec. III B). Finally, we propose a *coarse time-stepper* that mimics the evolution of the corresponding unavailable macroscopic model[8,9] (Sec. III C).

A. A hierarchy of macroscopic state variables

As in the mean-field approximation, we introduce the coverage of species A, $a(t)$, see Eq. (1), as the first macroscopic state variable. In addition, we introduce a hierarchy of macroscopic state variables M_A^l, $1 \leq l \leq L_A$, (respectively M_X^l, $1 \leq l \leq L_X$), of which each is defined as the number of clusters of particles A (respectively X) of *exactly* length l

$$\begin{aligned} M_A^l &= \frac{1}{2^{l+2}}\sum_{n=1}^{N}(\sigma_{n-1} - 1)(\sigma_{n+l} - 1)\prod_{k=0}^{l-1}(\sigma_{n+k} + 1), \\ M_X^l &= \frac{1}{2^{l+2}}\sum_{n=1}^{N}(\sigma_{n-1} + 1)(\sigma_{n+l} + 1)\prod_{k=0}^{l-1}(\sigma_{n+k} - 1), \end{aligned} \tag{4}$$

where periodic boundary conditions on the index n are assumed. The complete macroscopic state is then

$$\mathbf{M}_{L_A,L_X} = \left\{a, M_A^1, \ldots, M_A^{L_A}, M_X^1, \ldots, M_X^{L_X}\right\},$$

with maximum lengths L_A (respectively L_X).

Note that the above definition is slightly different from cluster-based definitions in the literature, such as the Kirkwood approximation[26] in which a cluster of length, e.g., $L_{\{A,X\}} = 3$ would be counted simultaneously as two clusters of length 2. In contrast, we only count structures of the form *AXXA* to determine the number of clusters of length 2. We introduce the notation

$$\langle XXX\rangle_{\boldsymbol{\sigma}} = \frac{1}{2^{l+2}} \sum_{n=1}^{N} \prod_{k=0}^{l-1} (\sigma_{n+k} - 1), \tag{5}$$

to denote the number of lattice sites occupied by species X, and also surrounded by species X, as it would appear in the Kirkwood approximation.

As will become clear in Sec. III B, this hierarchy of macroscopic state variables greatly simplifies the implementation of a consistent lifting strategy, without introducing additional complexity into the restriction.

B. Lifting and restriction

We introduce two operators that make the transition between microscopic and macroscopic state variables. We define a *lifting operator*,

$$\mathcal{L} : \mathbf{M}_{L_A,L_X} \mapsto \boldsymbol{\sigma}, \tag{6}$$

which maps a macroscopic state to a realization of a chain of length N, and an associated *restriction operator*,

$$\mathcal{R} : \boldsymbol{\sigma} \mapsto \mathbf{M}_{L_A,L_X}, \tag{7}$$

which maps a microscopic realization to the corresponding macroscopic state. The restriction operator is readily defined using Eq. (4).

The lifting step, however, is more involved. Besides, an obvious consistency condition, i.e.,

$$\mathcal{R} \circ \mathcal{L} \equiv \mathrm{Id},$$

one also needs to ensure that microscopic configurations that result from lifting do not contain undesirable artifacts, and actually represent realistic microscopic configurations. To this end, we introduce a *dynamical equivalence* concept to compare microscopic configurations. For the reaction laws (2), we say that two microscopic configurations $\boldsymbol{\sigma}_1$ and $\boldsymbol{\sigma}_2$ are dynamically equivalent, $\boldsymbol{\sigma}_1 \equiv \boldsymbol{\sigma}_2$, if they have the same number of possibly reacting lattice sites for each of the possible reactions, i.e., if

$$\begin{aligned} \langle XXX\rangle_{\boldsymbol{\sigma}_1} &= \langle XXX\rangle_{\boldsymbol{\sigma}_2}, \\ M_A^1(\boldsymbol{\sigma}_1) &= M_A^1(\boldsymbol{\sigma}_2), \\ a(\boldsymbol{\sigma}_1) &= a(\boldsymbol{\sigma}_1), \end{aligned} \tag{8}$$

where the notation in the first equality needs to be understood in the Kirkwood sense (5). The last two conditions are satisfied for microscopic configurations that have the same macroscopic state, for any L_X and $L_A \geq 1$, while the first condition is satisfied exactly only by conserving all the clusters (for instance, by choosing $L_X = L_A = N$). In this case, lifting corresponds to a random shuffle of clusters, and we have

$$\boldsymbol{\sigma} \equiv \mathcal{L}(\mathbf{M}_{N,N}(\boldsymbol{\sigma})). \tag{9}$$

When decreasing the number of macroscopic state variables, lifting will not preserve the numbers of longer clusters. Instead, we only conserve the *total number of elements of species X*, r_X, and of species A, r_A, *not contained within the counted clusters*, given by

$$\begin{aligned} r_A &= a\,N - \sum_{l=1}^{L_A} l M_A^l, \\ r_X &= (N - a\,N) - \sum_{l=1}^{L_X} l M_X^l. \end{aligned} \tag{10}$$

These remainders can be treated in a number of ways, each corresponding to an implicit choice of closure.

The investigation of different choices for the lifting is exactly the focus of the present paper. In particular, the main goal is to investigate which lifting operator recovers the macroscopic dynamics of the system with a minimal number of macroscopic variables.

C. The numerical closure algorithm

We are now ready to formulate the numerical closure algorithm. Given an initial condition for the macroscopic state variables $\mathbf{M}(t^*)$ at time t^*, we define *coarse time-stepper* as the following three-step procedure:

(i) *Lifting*, i.e., the creation of initial conditions

$$\boldsymbol{\sigma}(t^*) = \mathcal{L}(\mathbf{M}_{L_A,L_X}(t^*)),$$

for the microscopic model, consistent with the macroscopic state $\mathbf{M}_{L_A,L_X}$ at time t^*.

(ii) *Simulation* of the evolution of the microscopic state over a time interval $[t^*, t^* + \delta t]$ using the kMC null-event algorithm.

(iii) *Restriction*, i.e., the observation (estimation) of the macroscopic state at $t^* + \delta t$:

$$\mathbf{M}_{L_A,L_X}(t^* + \delta t) = \mathcal{R}(\boldsymbol{\sigma}(t^* + \delta t)).$$

To assess the effects of lifting on macroscopic evolution, we compare the time series of the macroscopic state variables $\mathbf{M}_{L_A,L_X}$ obtained via the numerical closure algorithm with those obtained by a complete microscopic simulation, $\mathbf{M}_{L_A,L_X}(t) = \mathcal{R}(\sigma(t))$. A similar study has been performed for a model for polymeric fluids.[27]

IV. LIFTING PROCEDURES

Let us now describe the principle underlying each of the specific lifting operators that we propose in this paper; for a detailed description, see the Appendix. Each lifting operator consists of two steps: (i) positioning of the conserved clusters of species X and A, as specified by the macroscopic state

variables $\mathbf{M}_{L_A,L_X}$; and (ii) distribution of the remaining r_A (respectively r_X) elements of species A (respectively X) grouping them in C_A (respectively C_X) blocks.

1. **lift**$_A$: Given r_A and r_X, we generate as many blocks of A and X as possible. These blocks then are necessarily short (but longer than those contained in the macroscopic state variables). As the number of blocks of A and X are not necessarily equal, several short blocks of the same species are likely to be concatenated, creating longer blocks.
2. **lift**$_B$: Instead of generating as many blocks as possible, a more realistic number of clusters is computed. To this end, we use the constraint that the total number of clusters for both species is necessarily equal to obtain a bound for the minimal and maximal number of clusters. We then generate a random number of clusters between these bounds.
3. **lift**$_C$: Often, the computed lower bound in **lift**$_B$ is very conservative, leading to clusters which are artificially long. To avoid this, we heuristically derive a reasonable maximal cluster length for given r_X and r_A based on a probabilistic reasoning. The minimal number of clusters $C_{A,X}^{\min}$ then follows.

Remark 4.1 (Lifting based on coverage). As a sanity check, we also consider a lifting based on only coverages. When choosing $L_A = L_X = 0$, the only macroscopic state variable is the coverage a, i.e., $\mathbf{M} = \{a\}$. In that case, the lifting generates a configuration $\boldsymbol{\sigma}$ in which the position of the $N \times a$ elements of species A is completely random. This method is labeled as **lift**$_R$.

V. NUMERICAL EXPERIMENTS

In this section, we illustrate the effects of the different lifting operators defined above. We apply them on the two examples introduced in Sec. II, analyze and quantify the deviations from the original microscopic simulations and discuss the observed discrepancies. All numerical results have been verified to be robust with respect to variations in the generated random numbers.

A. Example 2.1

We study the system (2) with two different reaction rates sets: $K_1 = [k_1 = 2, k_2 = 1, k_3 = 0.1, k_4 = 0.01]$ and $K_2 = [k_1 = 1, k_2 = 2, k_3 = 0.01, k_4 = 0.1]$. In both cases, the single-element reactions are slower than the reactions including nearest-neighbor interactions. The choice of these specific parameter sets is motivated by the differences in the resulting equilibrium values. For the reaction rates K_1, the concentration at equilibrium is $a_{\text{eq}} \simeq 0.9$; for the reaction rates K_2, is $a_{\text{eq}} \simeq 0.35$, see Figure 1. Unless otherwise stated, all simulations are performed on a lattice with $N = 2000$ sites for a time interval $T = [0, 400]$. We show in Secs. V A 1–V A 6 how the different equilibrium values effect the quality of the various liftings. We first assess the accuracy of the lifting procedure **lift**$_R$ whose macroscopic description is solely based on coverages (Sec. V A 1). We then introduce the augmented macroscopic variables set (Sec. V A 2) and perform

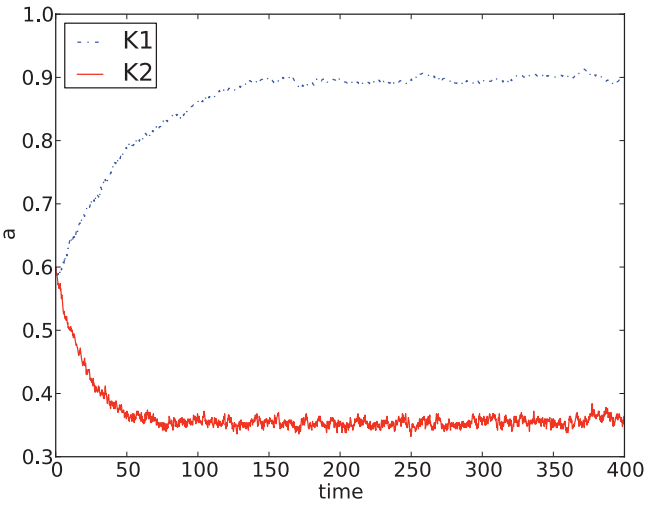

FIG. 1. Results for the microscopic dynamics for $K = K_1$ and $K = K_2$ reaction rates.

a numerical test using each of the discussed lifting strategies (Secs. V A 3–V A 5). The test consists of simulating using the coarse time-stepper using the minimal possible time step. Hence, after every microscopic time step, we first restrict to the selected macroscopic state variables, after which we lift back to a microscopic configuration. As a result, the observed macroscopic time evolution will mimic the numerical closure approximation induced by the lifting operator. Finally, we analyze the dynamics generated by these algorithms for larger and larger coarse time-steps (i.e., increasing the time between liftings), we will discuss the effects and limitations of the "healing principle" in this context (Sec. V A 6).

1. Coverage is insufficient as macroscopic state variable

We first present results using the coverage a as the only macroscopic state variable, from which we lift using the procedure **lift**$_R$. The numerical results, shown in Figure 2, indicate a significant deviation of the dynamics and the equilibrium. In fact, we obtain the mean field dynamics. This result is not surprising: when taking into account only the coverages, and randomly placing the elements of species A, one is in fact stirring the system, so spatial correlations are lost, and the system displays mean field behavior.

It has been argued[12] that errors in the macroscopic evolution that are induced by an incorrect microscopic initial condition may be able to "heal" by taking a larger coarse time step δt. Therefore, we enlarge the size of the coarse time step. Figure 2 shows that this leads to an improved agreement. However, for our system, the healing effect does not suffice for good macroscopic evolution. Obviously, using only the coverages as macroscopic variables does not seem to be, generally speaking, a good starting point for lattice reactive systems.

2. Selection of macroscopic state variables

Given the results from Sec. V A 1, we augment the set of macroscopic state variables which in turn induces the necessity to choose a more sophisticated lifting procedure

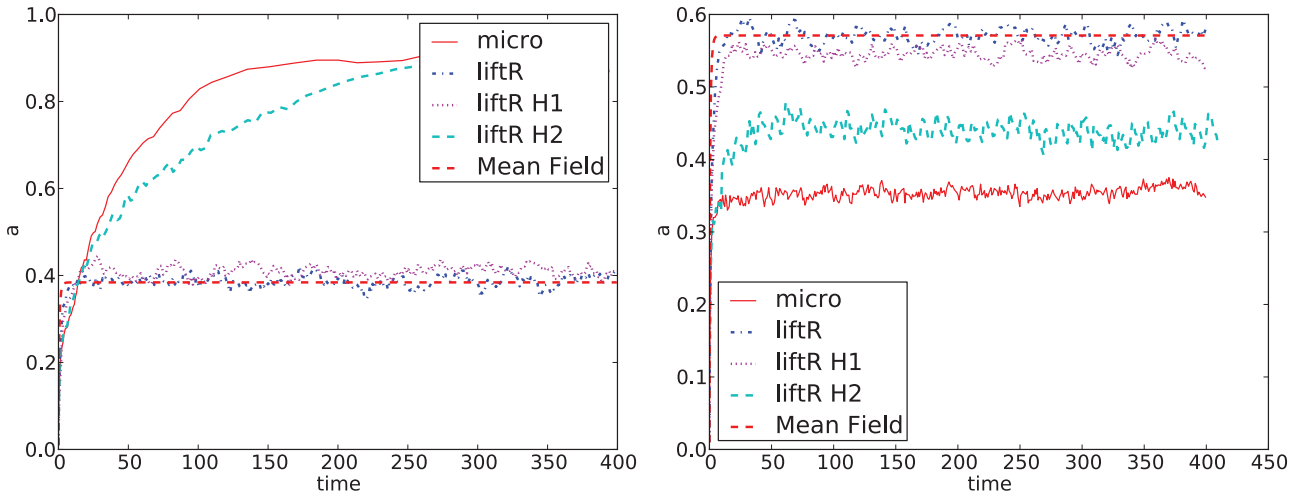

FIG. 2. Failure of healing, results for $\mathbf{lift}_R$ for examples 2.1 with $K = K_1$ (left) and with $K = K_2$ (right). The results refer to runs with 1000 microscopic time steps as coarse time stepper between every lifting/restriction procedure (H_1) and with 10 000 microscopic time steps (H_2). The total simulation time was 300 000 steps.

(as discussed above). As a first sanity check for the methodology, we initially perform a simulation with the coarse time-stepper using a very high number of macroscopic state variables, i.e., $L_X = L_A = N/20$. Obviously, in this case we perform almost no reduction, in the sense that only a few microscopic configurations are consistent with the considered macroscopic state. Figure 3 shows the results for both selected sets of reaction rates in the case of for $\mathbf{lift}_B$, equivalent results were obtained with the other lifting procedures but are not shown here. As expected, the agreement with the full microscopic simulations is almost perfect in this case. Our objective here is however to find the simplest (and most effective) algorithm that correctly reproduces these simulations. In this context, one will want to determine and use the smallest possible set of macroscopic variables for the corresponding coarse time-stepper. We propose to base this choice on the previously introduced dynamical equivalence, which in our sense is a good measure of the instaneous "reactivity" of a system.

Remember that we have considered two microscopic configurations to be equivalent if in both configurations, every reaction in the system is equally likely, i.e., in both configurations, there is an equal amount of reactive elementary blocks, see Eq. (8). For the chemical reactions (2), we observe that the first reaction introduces a dependence on the neighboring sites, while the second one does not. Consequently, when choosing L_A and L_X we focus on preserving the number of possible reactants of the first reaction, as the possible reactants for the second reaction are already determined by the coverages.

Let us first decide upon L_A. In particular, we note that isolated As are the only possible elements which may be modified by the first reaction. Therefore, we choose $L_A = 1$. The choice of L_X is more difficult, as one can never preserve the number of elements X which are surrounded by Xs, unless L_X is very large. However, we anticipate (and will show later on) that by keeping $L_A = 1$, while increasing L_X, we should be able to get to the smallest set of macroscopic variables

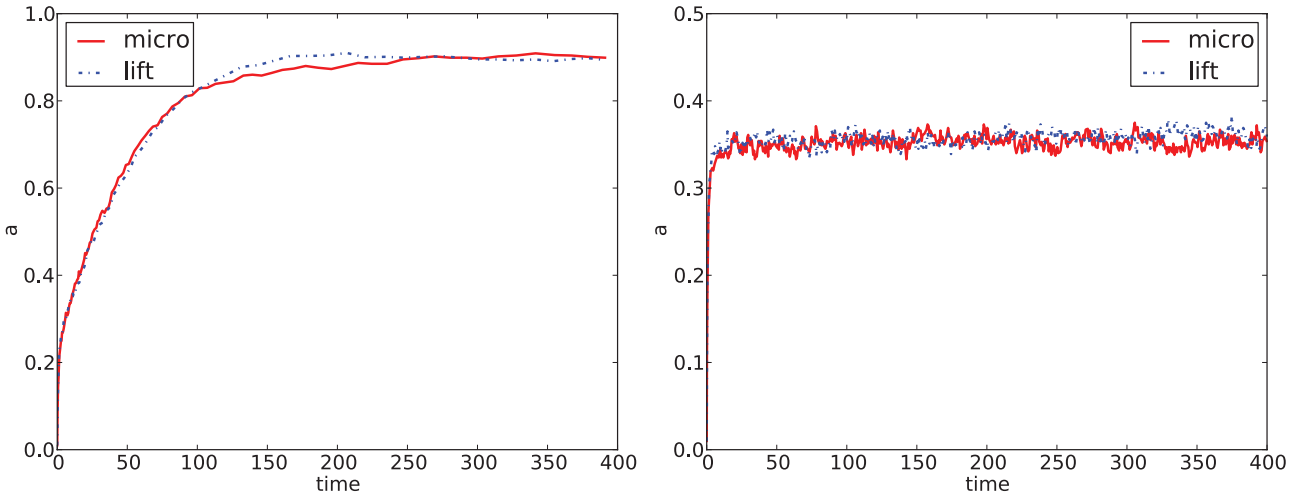

FIG. 3. Comparison of microscopic (continuous line) and restriction/lifting (dashed line) runs with $L_A = 100 = L_X = 100$. The results shown are for reaction rate K_1 (left) and K_2 (right). The runs refer to $\mathbf{lift}_A$, but equivalent results are obtained for the other lifting methods.

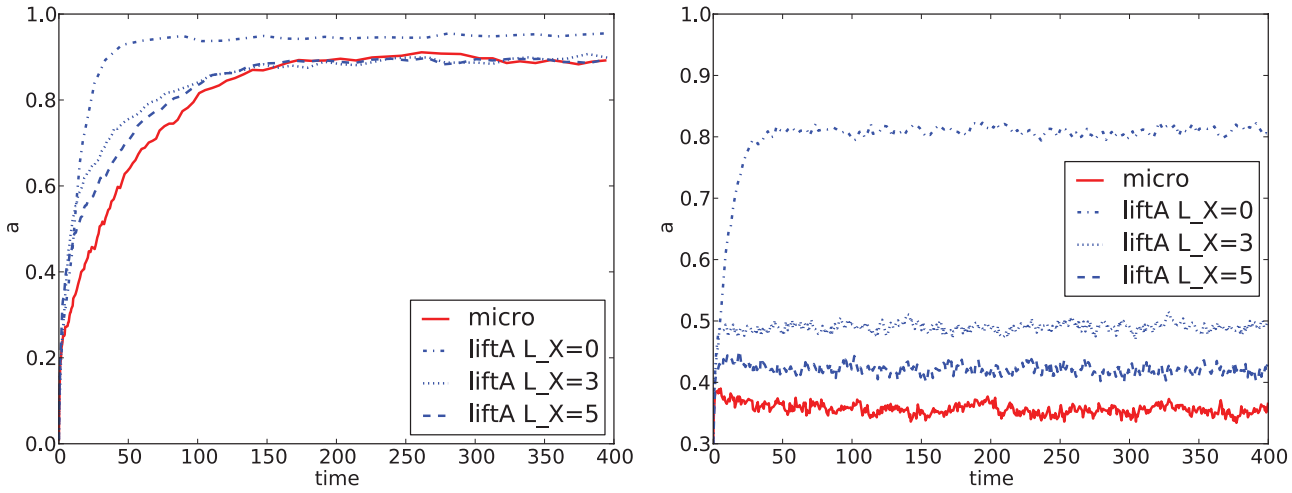

FIG. 4. Restriction/lifting results for $\mathbf{lift}_A$ for both sets of reaction rates $K = K_1$ (left) and $K = K_2$ (right). Comparison between different choices of L_X.

for which the coarse time-stepper recovers the macroscopic dynamics of the original microscopic system. For small values of L_X, we will show that the quality of the recovered macroscopic dynamics depends on the specifics of the lifting operator.

3. Lifting technique $\mathbf{lift}_A$

We now proceed by performing a simulation using the coarse time-stepper with the lifting $\mathbf{lift}_A$, using $L_A = 1$ and different values of L_X. The results for both sets of reaction rates (K_1 and K_2) are shown in Figure 4 for the smallest possible coarse time step. For the set of reaction rates K_1, when increasing L_X, we quickly obtain an excellent agreement between the numerical closure approximation and the fully microscopic simulation. For the set of reaction rates K_2, however, we see that for similar values of L_X, the macroscopic evolution behaves completely differently (both dynamically and in equilibrium), and we need to increase L_X quite substantially before getting an agreement.

This difference can be explained by analyzing the distribution of cluster size before and after the lifting. To this end, we start from an equilibrium microscopic configuration for a ring of length $N = 2000$ and count the number of clusters M_A^l and M_X^l ($l = 1, \ldots, N$) via Eq. (4) at each time step during a microscopic simulation, for a total time of $T = 100$ and average over time,

$$\overline{M_A^l} = \left\langle M_A^l(t) \right\rangle_{\text{eq}}, \quad \overline{M_X^l} = \left\langle M_X^l(t) \right\rangle_{\text{eq}},$$

where the subscript eq emphasizes the fact that the time average is taken over a simulation that is in equilibrium for all values of t. The resulting (normalized) histogram is plotted in Figure 5 (red starred line).

Next, to obtain a probability distribution for the coarse time stepper, we repeat the lifting procedure 10 000 times using method $\mathbf{lift}_A$, starting from the macroscopic state variables M_A^1 and M_X^l ($1 \le l \le L_X$), for different values of L_X, and average again the number of clusters of length $1 \le l \le N$ over the ensemble of microscopic configurations (see Figure 5). For

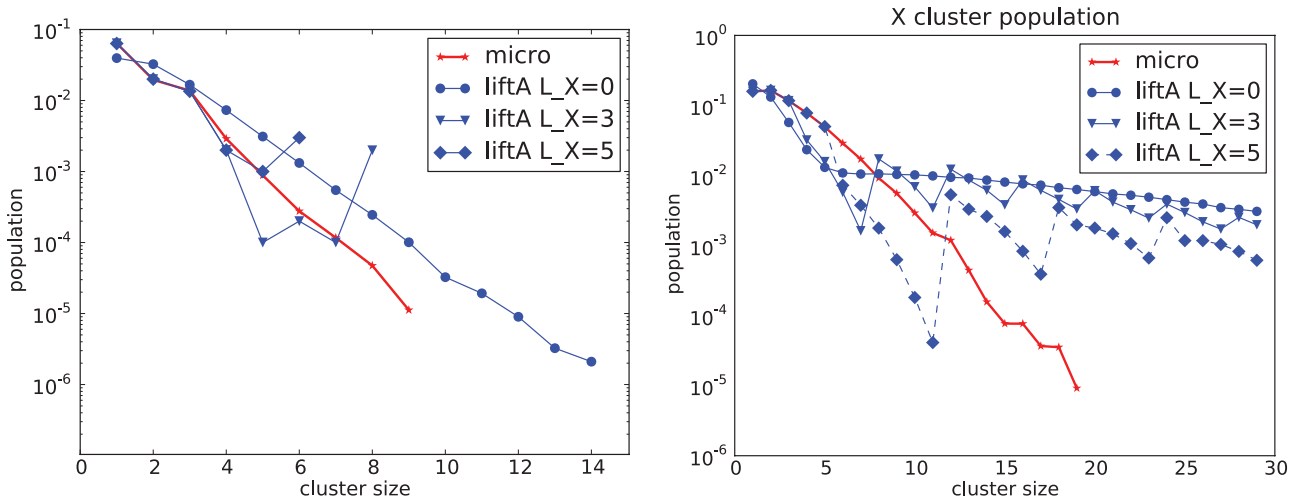

FIG. 5. Comparison of cluster populations for species X for $\mathbf{lift}_A$ at equilibrium in a semilogarithmic scale. The red stars correspond to the average over a microscopic run at equilibrium for $K = K_1$ (left) and $K = K_2$ (right). The other data correspond to the average of 10 000 liftings, given the values of the macroscopic set at equilibrium.

the original microdynamics, this distribution decays exponentially with the length of the clusters. Such rapid decrease can be explained by observing the reaction laws (2). Any long sequence of X is likely to be broken in two smaller ones by both reactions, while sequences of As can be interrupted only by the second reaction, so the dynamics greatly favors short clusters of Xs rather than longer ones. This feature is not preserved by the lifting procedure; as can be seen in Figure 5, for the lifted distributions, longer clusters are much more likely than for the microdynamics. Moreover, we also observe oscillations in the different cluster populations depending on the choice of L_X which determine the size of the blocks that are created with the remainders r_X.

While appealing due to its simplicity, the $\mathbf{lift}_A$ procedure thus suffers from some major drawbacks that can be related to its inability to correctly preserve the distribution of clusters size. It is relevant at this stage to identify the reasons behind this inaccuracy. Recall that in $\mathbf{lift}_A$, the idea is to maximize the number of clusters of species A and X created with the remainders, but that no special attention is being paid to their relative value. As a result, in the final step of the lifting, multiple building blocks of the same species can be selected, resulting in longer clusters. To analyze the lifted distributions, we need to estimate the probability of picking in sequence k blocks corresponding to species X from the remaining. For small values of k, relative to the total number of available blocks, i.e., $k \ll n^r$, this probability can be approximated by a simple multiplication of the probability of picking first a block of A then k blocks X and then another block X:

$$\mathcal{P}_k \simeq p_X^k (1 - p_X)^2 n^r, \tag{11}$$

where $p_X = \frac{C_X}{n^r}$ is the probability of getting a block of Xs out of the whole set. Using (11), and considering that the cluster population is simply $k\mathcal{P}_k$, we see that if $p_X \simeq 0.5$, i.e., we have approximately equally many building blocks for both species, then we get almost a plateau in the populations for clusters of length slightly larger than L_X. In Figure 5 we see such a plateau when $L_X = 0$. Remember that in this case, all elements of species X are in the remainder r_X as $\mathbf{M}_{L_A,0}$ carries no information about X clusters. When choosing $L_X > 0$, the behavior is different. In that case, we observe oscillations, which can be explained by noting that clusters are built by concatenation of building blocks, and hence, multiples of $L_X + 1$ are more likely to occur.

Increasing L_X gives better results because the number of building blocks of species X in the remainder decreases while the size of those blocks increases.

4. Lifting technique $\mathbf{lift}_B$

We now repeat the previous experiment for the lifting operator $\mathbf{lift}_B$, thus starting with the minimum coarse time step. For the reaction rates K_1, we observe a much better agreement with the microscopic data for small values of L_X. Choosing $L_X = 1$ already gives excellent agreement, see Figure 6 (left). For K_2, instead, the results are at first glance somewhat surprising. In fact, we get a very good agreement between the coarse time-stepper and the microscopic simulation by using only $L_X = 0$ and $L_A = 1$. However, when we add extra macroscopic variables, the results initially worsen.

The main reason for this unanticipated behavior may be found by analyzing the dependence of the minimal and maximal possible number of clusters in the remainders ($C^{\min}_{\{X,A\}}$ and $C^{\max}_{\{X,A\}}$, see Eqs. (A3) and (A4) in the Appendix for the explicit formulation) on L_X and L_A. We observe that a number $m_A - m_X$ of blocks of species A may be left over after placing all elements X coming from the macrovariable. These elements need to be placed in the final step of the lifting, together with the remainders of species X. For fixed L_A, the number $m_A - m_X$ reaches its maximum at $L_X = 0$, so $C^{\min}_X$ is maximal for $L_X = 0$. Simultaneously, because of the fact that all the elements of species X present in the system are contained in r_X, $C^{\max}_X$ is maximal for $L_X = 0$. A high value for $C^{\min,\max}_X$ implies that the elements of species X will be distributed in a large number of short clusters, which corresponds (by coincidence) to the structure of the microscopic realizations.

When $L_X > 0$, the quantity $m_A - m_X$ decreases, and so does $C^{\min}_X$, until it reaches its minimum value of 1, corresponding to a case in which all remaining elements of species

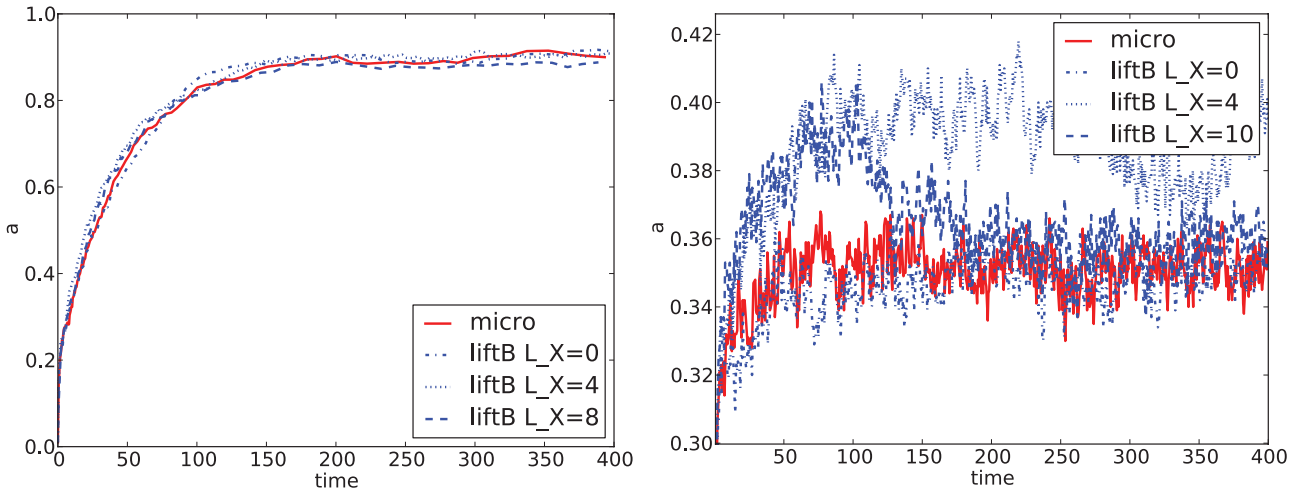

FIG. 6. Restriction/lifting results for $\mathbf{lift}_B$ for both sets of reaction rates K_1 (left) and K_2 (right); the figure on the right is zoomed to the equilibrium region.

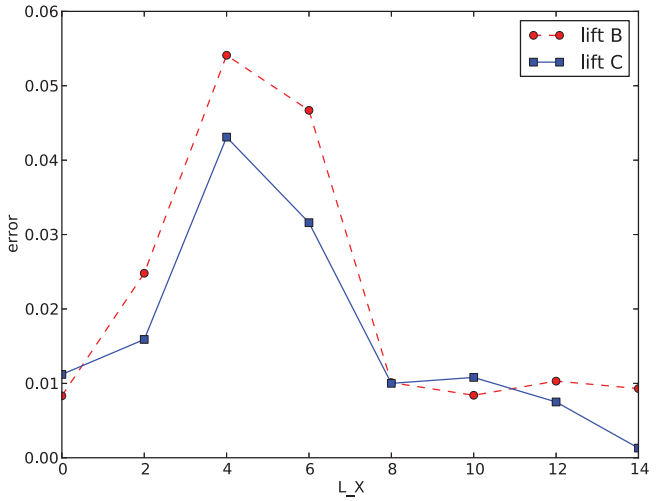

FIG. 7. Effect of increasing L_X using $\mathbf{lift}_B$ and $\mathbf{lift}_C$ when $K = K_2$. The error represents the time average of the square difference between the a coverage data coming from a microscopic run and a lifting/restriction one with initial conditions at equilibrium.

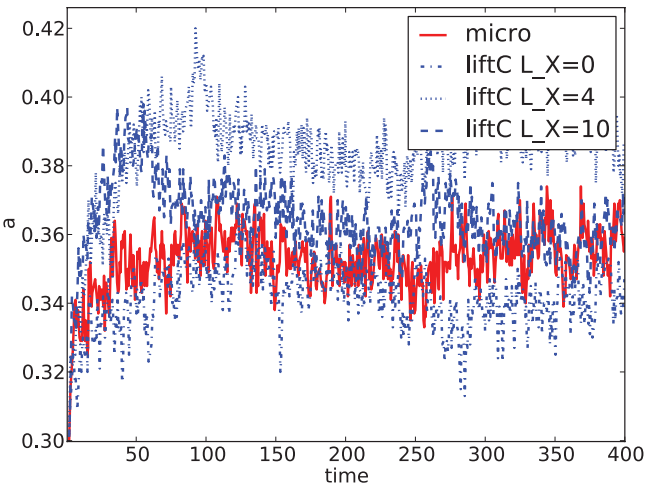

FIG. 9. Restriction/lifting results for $\mathbf{lift}_C$ and $K = K_2$.

X are contained in a single long cluster. (Note that, theoretically, one may also encounter situations in which $r_X = 0$ is empty, corresponding to $C_X = 0$.) It is then that we observe the largest error for the lifting. After this peak, the lifting performs better, as the number of elements in r_X decreases, leaving less room for artifacts in the evolution (Figures 6 and 7). As for $\mathbf{lift}_A$, we have evaluated the X cluster population at the equilibrium for $K = K_2$ and the results, shown in Figure 8 (left), are in line with the above observations. We note that the decay in cluster populations as a function of cluster length now becomes non-oscillatory. Nevertheless, this decay is still slow compared to that observed in the full microscopic simulation.

To summarize, when increasing the number of macroscopic variables L_X, we have a competition between two opposite effects. On the one hand, as expected, taking into account more variables reduces the degrees of freedom that are affected by the lifting, increasing the accuracy. On the other hand, we observe that, for intermediate values of L_X, a bias is introduced (via $C_X^{\min}$ in this case) in the distribution of the reconstructed elements. Depending on the relative importance of these effects, convergence to the microscopic dynamics may be non-monotonic. Note that this does not explain the very good agreement for the case $L_X = 0$, which is coincidental, and appears to be caused by the fact that lifting errors that artificially generate clusters that are too short do not affect the macroscopic dynamics.

5. Lifting technique $\mathbf{lift}_C$

Finally, we repeat the experiment for the lifting operator $\mathbf{lift}_C$. The idea is here to use an estimate of the cluster size distribution to find an appropriate estimate for the minimum number of clusters: we may for example use (11) to get an estimate for the maximum length, from which such number can be deduced. We set $C_X^{\min} = \tilde{k}$, with $\tilde{k}$ such that

$$p_X^{\tilde{k}}(1 - p_X)^2 n^r < \epsilon, \tag{12}$$

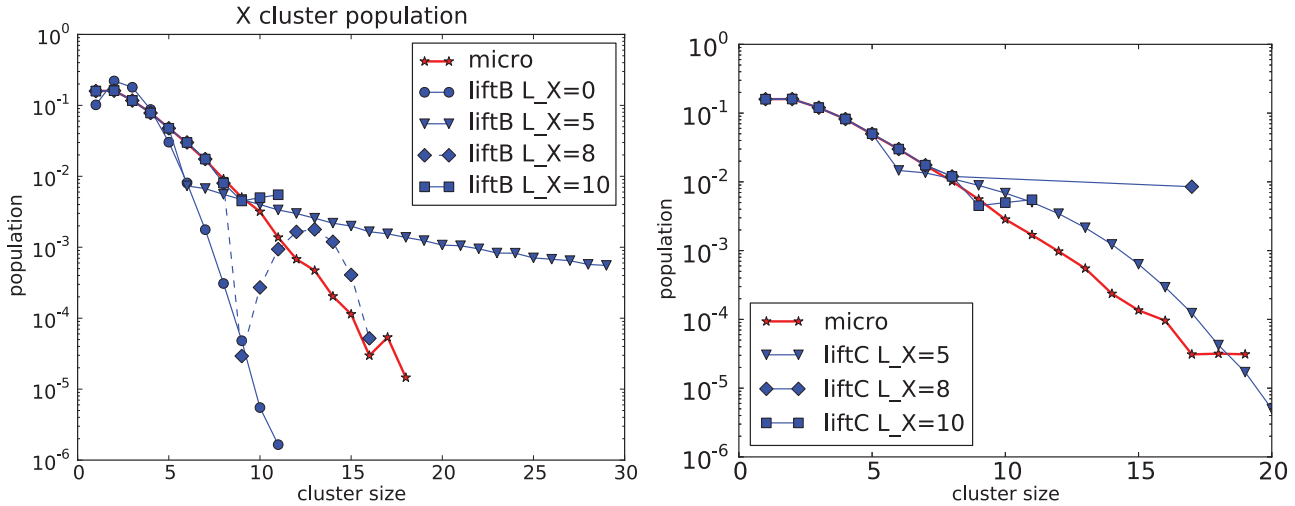

FIG. 8. Comparison of X cluster population for $\mathbf{lift}_B$ (left) and $\mathbf{lift}_C$ (right) at equilibrium in a semilogarithmic scale, the microdata refer to the average over a microscopic run at equilibrium for K_2, while the lifting are the repetition of 10 000 liftings given the values of the macroscopic set at equilibrium.

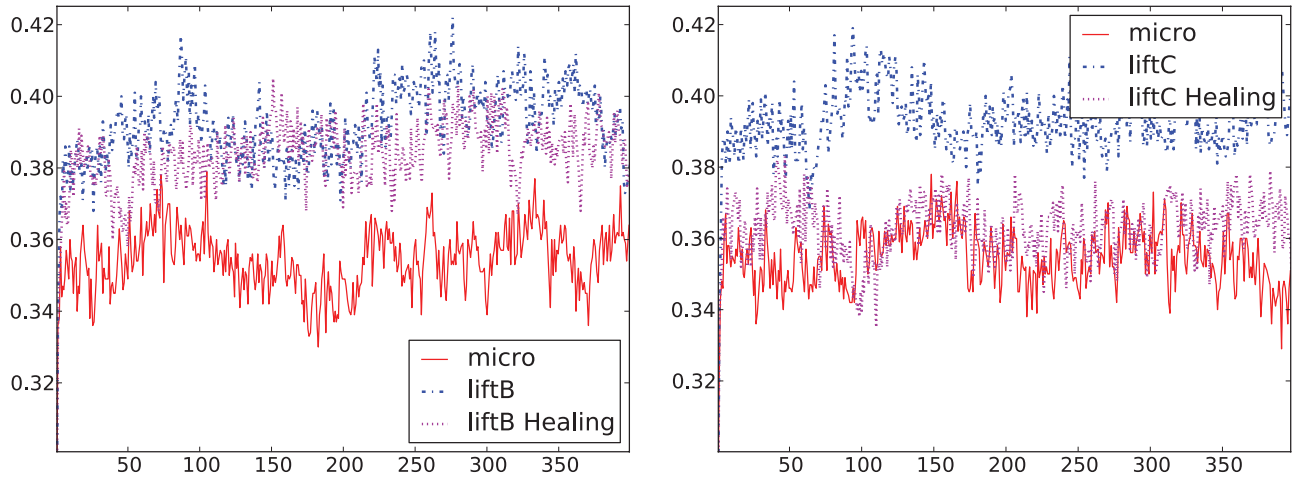

FIG. 10. Restriction/lifting results for $\mathbf{lift}_B$ (left) and $\mathbf{lift}_C$ (right) for $K = K_2$ with healing. In both the cases we compare the lifting procedure with and without healing (of 1000 microscopic time steps) The total simulation time is $T = 400$, 1000 steps correspond roughly to a time of 1. For the parameters we have $N = 3000$ and $L_X = 5$.

for a chosen small value of ϵ, explicitly excluding configurations that are very unlikely from a probabilistic point of view. (Here, we chose $\epsilon = 0.03$.) In our numerical experiments, the macroscopic simulation results for the reaction rates K_1 were very similar to those obtained with $\mathbf{lift}_B$. This is not surprising, as the lifting technique is similar in the sense that it also picks the number of clusters homegeneously between two imposed values, the only difference between these two schemes being in the estimate of the minimal number of clusters. We nevertheless notice that, for K_2, the results improve slightly (Figure 9). Considering again the distribution of cluster sizes (see Figure 8 (right)), we observe that some oscillations on the cluster populations are still present, but overall the distributions obtained with the liftings are closer to the data coming from the microscopic dynamics thanks to a better estimate for one of the boundaries in the number of clusters.

6. Effects of healing

As previously mentioned we have also checked the effect of the healing on the liftings $\mathbf{lift}_B$ and $\mathbf{lift}_C$ for those macroscopic variables sets which present the largest deviation from the microscopic dynamics, see Figure 10. Healing is expected to occur whenever a sufficiently long coarse time step is chosen. The two lifting procedures react in a quite different way to the increase of the coarse time step. We observe that even considering very large healing time, with $\mathbf{lift}_B$ we still do not recover the proper dynamics, instead for $\mathbf{lift}_C$ we observe a very good agreement using a healing time of the order of 1/300 of the total time. The reason for such result may again be founded on the fact that with $\mathbf{lift}_C$ the error on the cluster distribution for species X are smaller than with $\mathbf{lift}_B$ and such small error are corrected by short healing.

B. Example 2.2

Let us now turn to the simpler Example 2.2, in which only the nonlinear reaction is present. A direct microscopic simulation shows that a one-dimensional ring, initially completely covered by X evolves towards a macroscopic steady state with $a_{\text{eq}} \simeq 0.28$. If, instead, we look at the solutions of the approximating mean field equations, which may be easily written as $dx/dt = -x^3 + ax^2$, we obtain a steady state with equal concentrations of both species, and consequently $a_{\text{eq}} \simeq = x_{\text{eq}} = 0.5$. Obviously, a more sophisticated approach is here also necessary.

We first consider the lifting $\mathbf{lift}_R$, see Remark 4.1, which only takes into account the coverage of species A, and perform the same numerical experiment as for Example 2.1, see Sec. V A. The results are shown in Figure 11. We observe that, as expected, $\mathbf{lift}_R$ has $a = 0.5$ as steady state, demonstrating that this lifting induces the same closure approximation as the mean field equations.

A significant improvement can be obtained by making the following observation: if we start from a uniform X coverage, then any element of species A appearing in the ring is always necessarily surrounded by two elements of species X. Therefore, any cluster longer than a isolated A is physically

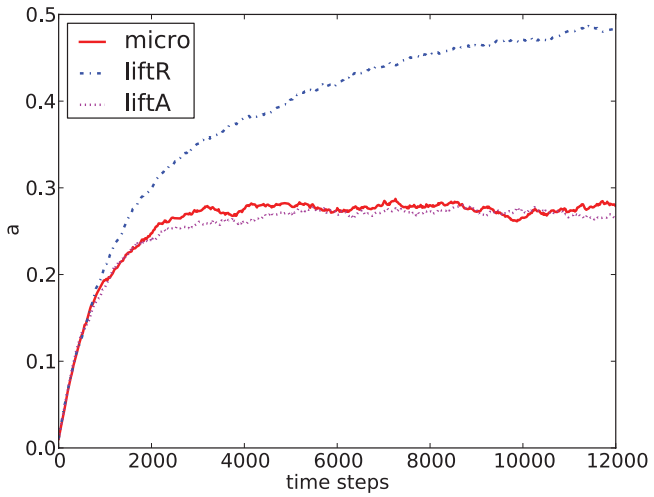

FIG. 11. Comparison of microdynamics with $\mathbf{lift}_R$ and $\mathbf{lift}_A$, both using $L_A = 0$, $L_X = 0$.

impossible. As a consequence, when we calculate the coverage, we are already calculating M_A^1, and we can easily take $\{a, M_A^1\}$ as the macroscopic variables set, instead of the sole coverage a. Note that, for this choice of macroscopic state variables, all lifting procedures introduced in Sec. IV become very similar. Indeed, for any value of L_X, the remainder of elements of species A that are not accounted for by the macroscopic state variables is empty ($r_A = 0$). The only choice that needs to be made is the division of the elements of r_X into clusters of different length that are necessary to separate all elements of species A. Here, we choose to simply separate each two elements of species A by a single cluster of species X of length $L_X + 1$. The remaining elements of species X are then inserted randomly next to an element of species A. We call the resulting lifting operator $\mathbf{lift}_A$.

The macroscopic dynamics that results from the coarse time-stepper is also depicted in Figure 11. The result illustrates that it is enough to take out the physically impossible states to get an excellent agreement between the microscopic and the coarse-grained dynamics. We reiterate that both liftings essentially start from the same macroscopic information, namely the number of elements of species A present in the system; the only difference is that, for $\mathbf{lift}_A$, we have used some additional information about the specific features of the microscopic dynamics, namely the fact that $a \equiv M_A^1$.

VI. DISCUSSION AND OUTLOOK

This paper introduced a new hierarchy of macroscopic state variables, and discussed and compared several numerical closure procedures based on these variables, based on a "dynamical equivalence" concept. We conclude by pointing out some directions for future research.

First, although we were able to identify efficient lifting strategies for the considered examples, it is not entirely clear how to develop a strategy in the more general case. Our results indicate that there exists a trade-off between the number of macroscopic state variables that one retains, versus the amount of effort that is put in the initialization of the remaining degrees of freedom of the system. An interesting approach would be to construct an approximate distribution of large clusters, based on the most popular analytical closure schemes (such as the Kirkwood approximation, the Ursell expansion, etc.) and then rely on the healing of the system during the coarse time step to correct the (hopefully) small errors introduced in this way. This approach would in addition allow one to formalize better the action of the lifting strategies and help choosing the best procedure, based on the known physical properties of the system. The efficiency of a particular choice of numerical closure is not only relevant for simulation purposes but also give important information on what closure relations make sense in the system under consideration. It is our opinion that the establishment of such a connection would open the way to a systematic numerical investigation of the level of accuracy of existing possible closures in stochastic systems.

Second, also the choice of macroscopic state variables is an active subject in multiscale simulation. While we have chosen a strategy based on an adaptive hierarchy of higher-order variables, other approaches, that identify the macroscopic state variables themselves based on fine-scale simulation, are currently also under investigation.[28,29]

ACKNOWLEDGMENTS

Y.D.D. and G.S. thank Yannis Kevrekidis for stimulating discussions. G.S. is a Postdoctoral Fellow of the Research Foundation–Flanders (FWO). The work of Y.D.D. was partially funded by the Fonds National pour la Recherche Scientifique (F.N.R.S.). This work was partially supported by the Research Council of KU Leuven through Grant No. OT/0927, by the Interuniversity Attraction Poles Programme of the Belgian Science Policy Office through Grant No. IUAP/V22.

APPENDIX: CONSTRUCTION OF THE LIFTING OPERATORS

In this section, we provide the technical choices that were made in the implementation of the lifting operators outlined in Sec. IV. Each lifting operator consists of two steps: (i) positioning of the conserved clusters of species X and A, as specified by the macroscopic state variables $\mathbf{M}_{L_A,L_X}$; and (ii) distribution of the remaining r_A (respectively r_X) elements of species A (respectively X).

The first step is common to all developed strategies, limiting differences in lifting operators to the distribution of the remainders. Each macroscopic state variable M_A^l ($1 \le l \le L_A$), respectively, M_X^l ($1 \le l \le L_X$), refers to the number of clusters of length l for species A, respectively X. We gather these clusters in two sets: $B_A = \{A, \ldots, A, AA, \ldots AA, AAA, \ldots, AAA, \ldots\}$, and similarly B_X, and then select elements from B_A and B_X alternatingly until one of the two sets is empty. We further introduce the notation

$$m_A = |B_A| = \sum_{l=1}^{L_A} M_A^l, \qquad m_X = |B_X| = \sum_{l=1}^{L_X} M_X^l,$$

for the cardinality of both sets. Since usually $m_A \neq m_X$, some elements from r_A or r_X will need to be used to ensure that we can place all clusters that are accounted for in the macroscopic state variables (see below). In the remainder, we assume that $m_X > m_A$, the argument for the alternative case is identical.

Given the definition of the macroscopic state variables, we need to group elements contained in the remainders r_A (respectively r_X) in blocks longer than L_A (respectively L_X). The lifting procedures described below differ exactly in the way these remaining elements are taken in account. As previously stated C_A (respectively C_X) represent the number of blocks containing only elements of species A (X respectively) which will be created with the r_A (respectively r_X) remaining elements. $\mathbf{lift}_A$, $\mathbf{lift}_B$, and $\mathbf{lift}_C$ consider different choices for C_A and C_X.

1. $\mathbf{lift}_A$: Given r_A and r_X, the largest number of blocks is defined by

$$C_X = \left\lfloor \frac{r_X}{L_X + 1} \right\rfloor \text{ and } C_A = \left\lfloor \frac{r_A}{L_A + 1} \right\rfloor.$$

Then, most of the C_A blocks of species A will have length $L_A + 1$; others will be longer because of the remainder of the division between r_A and $L_A + 1$. The same is true for the clusters of species X. Once these blocks have been created we have only to decide how to place them on the lattice. Having most of the blocks of equal length $L_X + 1$ may introduce artifacts on the distribution of clusters resulting from the lifting. To partially increase the randomness of such distribution we modify the equations for C_X and C_A by taking them to a random integer number picked by a uniform distribution between

$$\left(\frac{r_X}{L_X+2}, \frac{r_X}{L_X+1}\right) \text{ and } \left(\frac{r_A}{L_A+2}, \frac{r_A}{L_A+1}\right). \tag{A1}$$

In such way the length of the blocks is distributed more randomly.

2. **lift**$_B$: To generate a more realistic number of blocks we derive an upper and a lower limit for C_A and C_X, using the constraint

$$C_A + m_A = C_X + m_X. \tag{A2}$$

Then, the maximum number of clusters for species X can be derived to be

$$C_X^{\max} = \min\left(\left\lfloor \frac{r_X}{L_X+1}\right\rfloor, \left\lfloor \frac{r_A}{L_A+1}\right\rfloor + \max(m_A - m_X, 0) - \max(m_X - m_A, 0)\right), \tag{A3}$$

whereas for the minimum we have

$$C_X^{\min} = \max(\delta_{r_X}, m_A - m_X), \tag{A4}$$

where $\delta_{r_X} = 1$ if $r_X > 0$ and 0 otherwise; δ_{r_X} takes into account the unlikely event where all the elements X are contained into B_X. Similar formulas can be derived for $C_A^{\max}$ and $C_A^{\min}$. We then pick a number of clusters C_X randomly, based on a uniform distribution between the corresponding minimum and maximum, and infer the number of clusters C_A from (A2).

Once the numbers of clusters have been determined, and the corresponding individual clusters have been created, they need to be positioned on the lattice. Let us denote by B_A^r (respectively B_X^r) the sets containing the clusters built out of the remainders of each species. Recall that, given the assumption that $m_X > m_A$, we still need to place, besides the clusters corresponding to the remainders, $m_X - m_A$ clusters of species X corresponding to the macroscopic state variables. To this end, we continue as before, only now we alternatingly pick an element from B_X and B_A^r. After that step, for **lift**$_A$ the remaining $n^r := C_A + C_X - (m_X - m_A)$ clusters in $B_A^r \cup B_X^r$ are randomly picked and appended to the configuration; for **lift**$_B$ and **lift**$_C$ instead we have an equal number of elements remaining in B_A^r and B_X^r so it is sufficient to pick in the alternate way from the two sets. Note that from the cluster definition when reconstructing we impose adjacent clusters to superimpose at the head and the tail.

[1] G. Nicolis, Faraday Discuss. **120**, 1–10 (2002).
[2] A. V. Shabunin, F. Baras, and A. Provata, Phys. Rev. E **66**(3), 036219 (2002).
[3] V. P. Zhdanov, *Elementary Physicochemical Processes on Solid Surfaces*, Fundamental and Applied Catalysis (Plenum, 1991).
[4] D. T. Gillespie, J. Comp. Phys. **22**(4), 403–434 (1976).
[5] A. Chatterjee and D. Vlachos, J. Comput.-Aided Mater. Des. **14**, 253–308 (2007).
[6] M. Neurock, S. A. Wasileski, and D. Mei, Chem. Eng. Sci. **59**, 4703–4714 (2004).
[7] D.-J. Liu and J. W. Evans, J. Chem. Phys. **124**, 154705 (2006).
[8] Y. G. Kevrekidis, C. W. Gear, J. M. Hyman, P. G. Kevrekidis, O. Runborg, and C. Theodoropoulos, Commun. Math. Sci. **1**(4), 715–762 (2003).
[9] Y. G. Kevrekidis and G. Samaey, Annu. Rev. Phys. Chem. **60**, 321–344 (2009).
[10] W. E and B. Engquist, Commun. Math. Sci. **1**(1), 87–132 (2003).
[11] W. E, B. Engquist, X. Li, W. Ren, and E. Vanden-Eijnden, Comm. Comp. Phys. **2**(3), 367–450 (2007).
[12] A. G. Makeev, D. Maroudas, A. Z. Panagiotopoulos, and Y. G. Kevrekidis, J. Chem. Phys. **117**(18), 8229–8240 (2002).
[13] A. G. Makeev and Y. G. Kevrekidis, Surf. Sci. **603**(10–12), 1696–1705 (2009).
[14] C. W. Gear, T. Kaper, Y. G. Kevrekidis, and A. Zagaris, SIAM J. Appl. Dyn. Syst. **4**(3), 711–732 (2005).
[15] A. Zagaris, C. W. Gear, T. J. Kaper, and Y. G. Kevrekidis, ESAIM: Math. Modell. Number. Anal. **43**, 757–784 (2009).
[16] R. J. Glauber, J. Math. Phys. **4**(2), 294–307 (1963).
[17] A. Tretyakov, A. Provata, and G. Nicolis, J. Phys. Chem. **99**(9), 2770–2776 (1995).
[18] S. Prakash and G. Nicolis, J. Stat. Phys. **82**, 297–322 (1996).
[19] A. G. Makeev, D. Maroudas, and Y. G. Kevrekidis, J. Chem. Phys. **116**(23), 10083–10091 (2002).
[20] X. Guo, Y. De Decker, and J. W. Evans, Phys. Rev. E **82**, 021121 (2010).
[21] D. R. de Souza and T. Tomé, Physica A **389**(5), 1142–1150 (2010).
[22] A. Provata, J. W. Turner, and G. Nicolis, J. Stat. Phys. **70**, 1195–1213 (1993).
[23] R. M. Ziff, E. Gulari, and Y. Barshad, Phys. Rev. Lett. **56**, 2553–2556 (1986).
[24] S. Prakash and G. Nicolis, J. Stat. Phys. **86**, 1289–1311 (1997).
[25] E. Abad, P. Grosfils, and G. Nicolis, Phys. Rev. E **63**, 041102 (2001).
[26] J. W. Evans, D. K. Hoffman, and H. Pak, Surf. Sci. **192**, 475–450 (1987).
[27] G. Samaey, T. Lelièvre, and V. Legat, Comput. Fluids **43**(1), 119–133 (2011).
[28] B. Nadler, S. Lafon, R. R. Coifman, and Y. G. Kevrekidis, Appl. Comput. Harmon. Anal. **21**(1), 113–127 (2006).
[29] M. Belkin and P. Niyogi, Neural Comput. **6**(15), 1373–1396 (2003).

The Journal of Chemical Physics is copyrighted by the American Institute of Physics (AIP). Redistribution of journal material is subject to the AIP online journal license and/or AIP copyright. For more information, see http://ojps.aip.org/jcpo/jcpcr/jsp